Review of Scientific Instruments

A scalable high-performance magnetic shield for very long baseline atom interferometry

Cite as: Rev. Sci. Instrum. **91**, 035117 (2020); https://doi.org/10.1063/1.5141340
Submitted: 04 December 2019 . Accepted: 03 March 2020 . Published Online: 19 March 2020

E. Wodey, D. Tell, E. M. Rasel, D. Schlippert, R. Baur, U. Kissling, B. Kölliker, M. Lorenz, M. Marrer, U. Schläpfer, M. Widmer, C. Ufrecht, S. Stuiber, and P. Fierlinger

AIP Publishing

Review of Scientific Instruments ARTICLE scitation.org/journal/rsi

A scalable high-performance magnetic shield for very long baseline atom interferometry

Cite as: Rev. Sci. Instrum. 91, 035117 (2020); doi: 10.1063/1.5141340
Submitted: 4 December 2019 • Accepted: 3 March 2020 •
Published Online: 19 March 2020

E. Wodey,[1] D. Tell,[1] E. M. Rasel,[1] D. Schlippert,[1,a)] R. Baur,[2] U. Kissling,[2] B. Kölliker,[2] M. Lorenz,[2] M. Marrer,[2] U. Schläpfer,[2] M. Widmer,[2] C. Ufrecht,[3] S. Stuiber,[4] and P. Fierlinger[4]

AFFILIATIONS

[1]Leibniz Universität Hannover, Institut für Quantenoptik, Welfengarten 1, 30167 Hannover, Germany
[2]IMEDCO AG, Industriestrasse West 14, 4614 Hägendorf, Switzerland
[3]Universität Ulm, Institut für Quantenphysik and Center for Integrated Quantum Science and Technology (IQ^{ST}), Albert-Einstein-Allee 11, 89069 Ulm, Germany
[4]Technische Universität München, Physikdepartment, 85748 Garching, Germany

[a)]**Author to whom correspondence should be addressed:** schlippert@iqo.uni-hannover.de

ABSTRACT

We report on the design, construction, and characterization of a 10 m-long high-performance magnetic shield for very long baseline atom interferometry. We achieve residual fields below 4 nT and longitudinal inhomogeneities below 2.5 nT/m over 8 m along the longitudinal direction. Our modular design can be extended to longer baselines without compromising the shielding performance. Such a setup constrains biases associated with magnetic field gradients to the sub-pm/s^2 level in atomic matterwave accelerometry with rubidium atoms and paves the way toward tests of the universality of free fall with atomic test masses beyond the 10^{-13} level.

I. INTRODUCTION

Light pulse atom interferometers are powerful tools for modern precision metrology.[1–3] They exploit the fine and well understood control of matter waves by light to achieve record instabilities and inaccuracies in the precision measurement of forces and other inertial quantities.[4–9] In the conventional Kasevich–Chu geometry,[10] the phase sensitivity of these interferometers scales linearly with the enclosed space-time area. By extending the free fall distance from tens of centimeters to the order of 10 m, large scale atom interferometers[11,12] target more than a factor of 50 increase in their scale factor. When applied to the measurement of the local gravitational acceleration, the combination of such long baselines with high-performance inertial reference platforms brings short-term instabilities competing with state-of-the-art superconducting gravimeters in reach while, in addition, providing absolute measurements.

However, spurious field gradients along the free evolution path of the atoms can mimic the signal of interest and, therefore, limit the measurement accuracy and instrumental stability. In particular, magnetic field inhomogeneities generate bias accelerations on the atoms due to the Zeeman effect. Magnetic gradients at the few nT/m level or better along baselines of several meters are, therefore, required to satisfy the accuracy budget of these large scale atom interferometers at the sub-nm/s^2 level, compatible with their target instability.[13] Magnetic shielding is typically achieved by channeling the external magnetic flux inside a high permeability shell around the volume to isolate.[14] Here, the homogeneity of the shielding material's permeability is key to ensure a uniform magnetization of the shield. This is, however, challenging on the lengths required by large scale atom interferometers since the production of homogeneous extended curved sheet metal is problematic, as well as the gap-free and reproducible junction of several pieces. A commonly used solution is to produce a fully welded assembly, which is subsequently hydrogen annealed to ensure homogeneous properties of the shielding material.[15] This is, however, impractical due to the limited availability of suitable furnaces and lacks scalability for future, possibly larger applications. Here, inspired by the layout

of magnetically shielded rooms,[16] we report on the design, construction, and characterization of a 10 m-long magnetic shield for the Hannover Very Long Baseline Atom Interferometry (VLBAI) facility.[13] We first describe the key design points in achieving a fully length-scalable, large length-to-diameter ratio magnetic shield which does not require overall annealing. We then assess the shield's performance with residual field and dynamical shielding factor measurements and finally discuss its application in precision atom interferometry.

II. SHIELD DESIGN AND CONSTRUCTION

In our atom interferometer, atoms fall freely inside a vertically oriented 10.5 m long aluminum ultra-high vacuum pipe[17] with an inner diameter of 18 cm and an outer diameter of 20 cm. The magnetic shielding enclosure for this cylindrical vacuum chamber consists of two concentric octagonal prism shells of high permeability Ni–Fe alloy[18] ("permalloy"), as shown in Fig. 1. The inner and outer permalloy shells have circumscribed diameters of 450 mm and 750 mm, respectively. Both shells are closed individually by end-caps, resulting in a total length of 9.7 m for the inner shell and 10 m for the outer one. The entire shielding assembly weighs around 7500 kg. On the main axis of symmetry, a 22 cm diameter circular opening is left in the end-caps as clearance for the vacuum chamber.

Despite the cylindrical symmetry of the volume to isolate, an octagonal geometry turned out to be more practical. It allows using mainly a planar sheet material with well-defined and homogeneous permeability after annealing, which enables more reliable finite element simulation of the assembly. Figure 2 shows the construction principle of the shielding enclosure. The octagonal prism shape is maintained by a structure made of 21 mm thick plywood. The plywood panels are assembled inside an extruded aluminum frame using aluminum fixtures and titanium and stainless steel bolts and nuts. The 1 mm thick annealed permalloy sheets are stacked and pressed against the supporting plywood structure by means of titanium wood screws. High pressure laminate (HPL) strips help distribute the load applied by the screws. Clearance holes for the screws in the permalloy sheets are laser cut after the annealing procedure. The gaps on the edges of the octagonal prism shape are closed using angled permalloy strips. The strips are bent after the annealing procedure. Angled and planar sheets are alternated, as shown in Fig. 2. In the longitudinal direction, the permalloy sheets are close to 3 m long. The few mm gap between consecutive planar sheets is bridged by offsetting the next sheet on the stack with 50% overlap, as shown in the inset of Fig. 2. In order to avoid saturation effects and help the magnetic equilibration field to penetrate effectively, the nominal thickness of the shells varies from 3 mm at the ends up to 8 mm in the central region. In Fig. 2, the transition between three planar sheets (nominal thickness of 3 mm) and five planar sheets

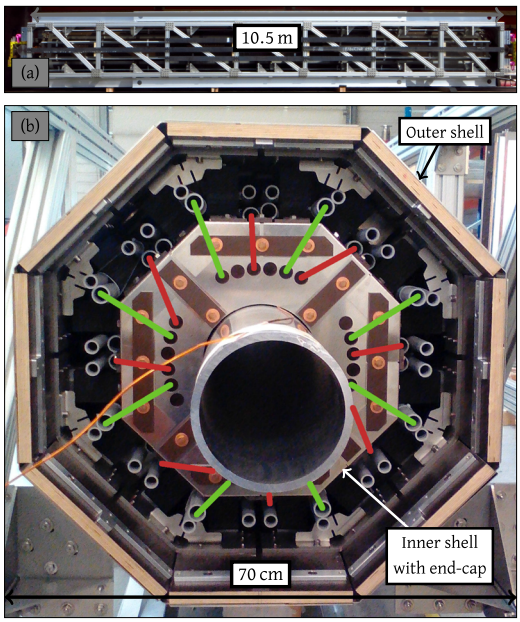

FIG. 1. Photographs of the assembled magnetic shielding enclosure. (a) Side view of the final assembly. (b) End view with the end-cap for the outer shell removed. Two octagonal prism permalloy shells are supported by a plywood structure. Between the shells, PVC pipes guide the magnetic equilibration coils. Red and green lines show the routing of the two coils used for the equilibration of the inner layer. In the center, an aluminum pipe holds the space for the interferometer's vacuum chamber.

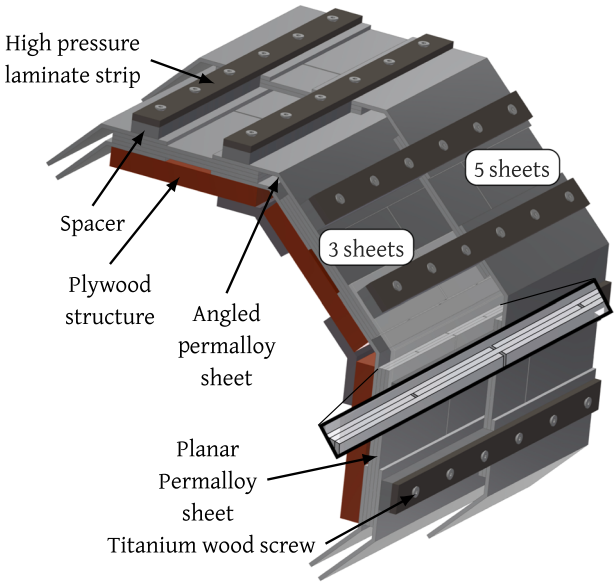

FIG. 2. Principle for the assembly of the permalloy sheets for a single shell (not to scale). The 1 mm thick permalloy sheets are stacked and pressed against a supporting plywood structure. Planar and angled strips are alternated. In the longitudinal direction, gaps between consecutive sheets (planar or angled) are closed by offsetting the next sheet layer, as shown in the inset. High pressure laminate (HPL) strips help distribute the load applied by the titanium wood screws. We use one screw every 250 mm to ensure uniform pressure on the permalloy sheets. Since the total nominal thickness of the shield varies along its length, polymer spacers are used to keep the HPL strip level, as shown here for the transition between three and five planar sheets (3–5 mm effective shell thickness).

(nominal thickness of 5 mm) is depicted. The four end-caps are built following the same principles as the main section of the shield. The connection between the end-caps and the main body is done by overlapping the extremities of the permalloy sheets from both parts over 20 cm and pressing them together against the plywood structure.

This construction allows for precise positioning of each sheet while keeping the material stress-free and hence reducing buildup of inhomogeneities in its magnetic permeability. It is, in particular, crucial that the mechanical robustness is given by the plywood structure and not by the shielding material itself. The plywood structure and the air gap between the layers also provide an electrical isolation over 10 MΩ. This design is also fully scalable in length. The permalloy sheet material is annealed before assembly on the plywood structure, making the largest pieces to anneal only 3 m long. This removes the need for a large hydrogen furnace,[15] irrespective of the final length of the shield. Finally, the possibility to open individual faces of the shells provides great access and flexibility for the installation of the vacuum chamber.

In order to minimize the free energy of the magnetic domains in the shielding material, we use a magnetic equilibration ("degaussing") procedure similar to the one described by Altarev *et al.*[16] We apply the equilibration field using coils routed around the faces of the octagonal prism shells with PVC pipes as guides (see Fig. 1). For the inner shell, we use two sets of five turns of 6 mm^2 copper wire connected in parallel, building up a coil enclosing each face of the permalloy octagonal prism twice (red and green lines in Fig. 1). The resistive impedance of the equilibration coils for the inner layer is around 2.5 Ω per coil. We connect these coils in parallel to relax the voltage requirements on the coil driver. For the outer layer, we use only a single pass per face with five turns of the same wire, which amounts to 2.7 Ω of resistive load. Finally, we set up another pair of coils for the end-caps with five turns of 2.5 mm^2 cross section wire per end-cap. These coils are wired in series and sum up to a resistance of 0.3 Ω. We drive the equilibration coils sequentially: first, for the inner shell, then the end-caps, the outer shell, and finally the inner shell again. Each step starts by feeding 6 Hz, 10 A rms sinusoidal current in the coil and then decreasing the peak current linearly over 100 s. The full equilibration sequence, therefore, lasts around 7 min. The target current waveform is calculated on a computer and fed into a 16-bit voltage output DAC that drives an offset-trimmed current-mode amplifier. Residual offsets at the output of the current amplifier are further reduced by using an external low distortion transformer.

III. MEASUREMENTS

We determine the dynamical shielding factors in the middle of the shield (Sec. III A) and the residual vector field along the full longitudinal axis (Sec. III B) using the setup shown in Fig. 3. The end-caps are fully closed on both sides. We effectively reproduce the conditions of the final experimental apparatus by using a replicate of the vacuum chamber's aluminum pipe as a guide for the magnetic field sensors. For practicality reasons, however, the shield is in the horizontal position, whereas it will be implemented vertically in the final configuration.

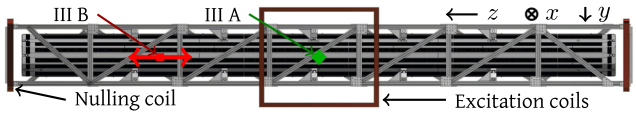

FIG. 3. Setup for the characterization measurements. In Sec. III A, we use three orthogonal coil pairs around a fixed probe in the middle of the shield (green filled diamond) to measure the dynamical shielding factors in all three spatial directions. For the residual field measurements in Sec. III B, the probe (red filled square) travels along the longitudinal axis (*z* direction) of the shield and we coarsely null the field at the ends of the shield using two constant current coils, while the excitation coils are not used.

A. Dynamical shielding factor

We first measure the response of the shield to a sinusoidal external field perturbation. We define the dynamical shielding factor as the ratio of the amplitude of the applied perturbation to the measured amplitude inside the shield.[16] We apply the external perturbation using a set of three calibrated rectangular coil pairs of dimensions 3 × 2 m^2 around the center of the shield. The resulting field in the corresponding frequency band is recorded by using a three axis fluxgate sensor placed in the middle of the shield. To avoid saturating the magnetometer's digitizer, we vary the applied field between 700 nT and 2000 nT. Figure 4 shows the measured dynamical shielding factor vs frequency for all three directions. In the transverse directions, the shielding ratio reaches values above 4000 at 0.01 Hz, similar to other two-layer designs.[16] The corresponding longitudinal damping is more than 100 times lower, as expected from the large length-to-diameter ratio.[15] Owing to the cancellation of the field's divergence in vacuum, the longitudinal field must be homogeneous if the transverse gradients are nulled and it can, therefore, be adjusted by a simple solenoid. Finally, we note that the change in the slope observed in all directions around

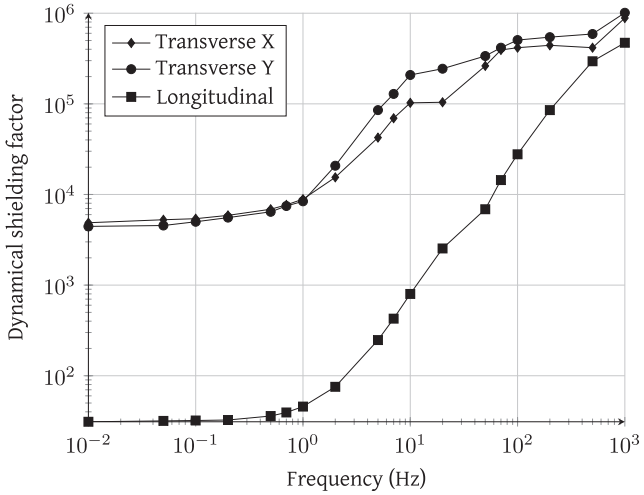

FIG. 4. Measurement of the dynamical shielding factor at the center of the shield with end-caps installed. Effective eddy current shielding the aluminum pipe used as a guide for the probe is visible through the increased shielding factor at frequencies above 1 Hz.

1 Hz is the characteristic of the crossover between effective shielding by the permalloy sheets at low frequencies (magnetostatic shielding) and by the aluminum pipe above this threshold (eddy current shielding[19,20]).

B. Residual field

We also map the three components of the residual field along the symmetry axis of the shield. We mount a three axis magnetometer[21] on a wooden mount assembled with non-metallic connectors to enable it to travel on the shield's axis guided by the aluminum pipe. We measure the position of the sensor in the shield using a remote controlled laser distance meter. We place two constant current loops around the end-caps of the magnetic shield to coarsely null the longitudinal field component near the entrance of the shield (Fig. 3). The shield is otherwise fully passive, and we, in particular, did not implement any active external field stabilization. The magnetometer's output signals are conditioned by commercial pre-amplifiers[22] and digitized using auto-zeroed 6.5 digit digital multimeters.[23] We perform six scans of the field on the shield's axis over two consecutive days. Each scan consists of ca. 90 points separated by ~10 cm to map the full 10 m of the shielded region. Each point is a 20 s average, corresponding to 50 acquisition cycles from the digital multimeters.[24] Since the probe offsets are only calibrated to ±5 nT in the factory, we perform a custom offset calibration step between all scans. For this, we measure both the parallel and antiparallel components of the field and take their average to find the probe offset. This is better realized in low field regions to limit errors due to imperfect inversion of the sensitive axis direction. We observe that measured offsets are reproducible at the 1 nT level and, therefore, attribute an uncertainty of ±500 pT to the absolute magnetic field measurements. We note, however, that probe offsets can vary more significantly when cycling the sensor's power or stressing readout connectors.[25] Finally, to account for the large variability of the external field, up to 400 nT peak-to-peak on the 1 h scale, due to industrial activity in the surrounding area, we also apply the equilibration procedure between each run. Figure 5 shows the measured field maps with a residual magnetic field below 4 nT over the inner 8 m of the shielded region. The reproducibility of the scans over 20 cm windows is better than 1.5 nT max-to-min and better than 500 pT on the standard deviation, demonstrating the robustness of the magnetic equilibration procedure.

IV. APPLICATION TO PRECISION ATOMIC ACCELEROMETRY

For our application in precision atom interferometry, the leading systematic error associated with magnetic fields is due to the Zeeman effect. For atomic states with zero magnetic quantum number, the linear component of the Zeeman effect vanishes and the potential seen by the atoms due to a longitudinal magnetic field profile $B(z)$ is quadratic in the total field strength,

$$V(z) = -\frac{1}{2}\hbar\alpha B(z)^2. \tag{1}$$

Here, $\hbar$ is the reduced Planck constant and α is the atomic species' clock transition Zeeman coefficient (57.5 GHz/T^2 for the ^{87}Rb atom[26]). Using perturbation theory,[27,28] we evaluate the phase ϕ of an atom interferometer in the presence of an arbitrary but small perturbation potential $V(z)$. To first order, we get

$$\phi = \phi_0 - \frac{1}{\hbar}\oint \mathrm{d}t\, V(z_0(t)), \tag{2}$$

where ϕ_0 is the phase of the corresponding unperturbed interferometer and the integral spans over the oriented loop formed by the unperturbed classical trajectories $z_0(t)$. In the presence of a local gradient with no curvature and writing the magnetic field profile as $B(z) = B_0 + \epsilon b(z)$, $\epsilon \ll 1$, the local bias acceleration on atoms of mass m reads

$$\delta a = \epsilon\frac{\hbar\alpha B_0}{m}\frac{\partial b(z)}{\partial z} + \mathcal{O}(\epsilon^2). \tag{3}$$

We numerically calculate the magnetic field gradient from the data of Fig. 5. The resolution is limited by the finite spatial sampling of the data. However, between all six scans presented in Fig. 5, the sensor positions were not exactly reproduced, making the sampling grid effectively finer than 10 cm. Moreover, due to smoothness requirements of the magnetic field, we do not expect spurious features to have been missed in the residual field measurement and, therefore, interpolate the data linearly and take

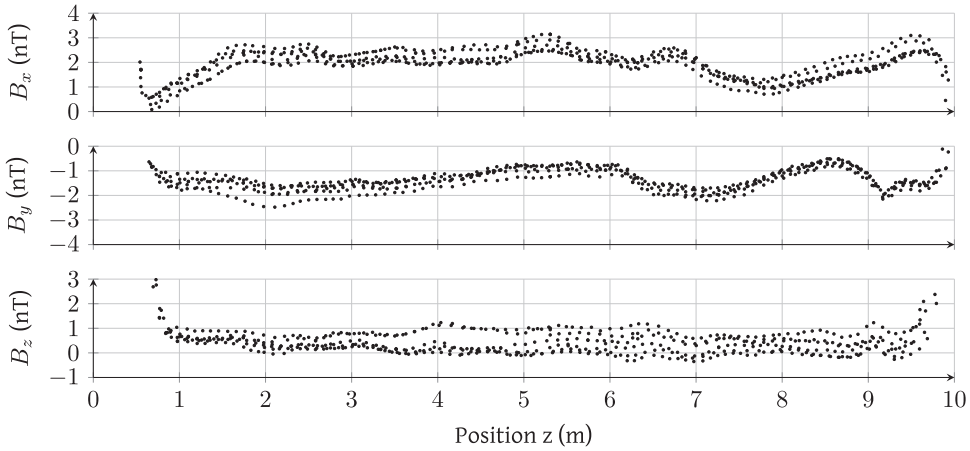

FIG. 5. Measurements of the residual magnetic field components along the shield's symmetry axis. The magnitude of the residual field does not exceed 4 nT over the inner 8 m with reproducibility better than 1.5 nT between scans. The directions x and y are transverse, while z is longitudinal. The data consist of 570 points from 6 full length scans distributed over two consecutive days with magnetic equilibration between the scans.

the local slope as the local gradient. Over the inner 8 m of the shielded region, the local longitudinal magnetic field gradient never exceeds 3 nT/m, which corresponds to a maximum local acceleration of 1.2 pm/s^2 for ^{87}Rb atoms when B_0 = 1.5 μT. This effect can be constrained further by applying the perturbation theory result of Eq. (2) since the integral over the unperturbed classical trajectories smoothes local spikes in the magnetic field profile. For a simple drop mode operation, we find the bias for an interferometer spanning the inner 8 m of the shielded region to be smaller than five parts in 10^{15} of the Earth's local gravitational acceleration.

V. CONCLUSION

We reported on the design, construction, and characterization of a 10 m high-performance magnetic shield with application in very long baseline atom interferometry, achieving residual fields below 4 nT and longitudinal gradients smaller than 2.5 nT/m over the central 8 m. Owing to the use of the pre-annealed permalloy sheet material in an octagonal prism geometry and careful, stress-free assembly, the design is fully scalable in length, effectively removing the need for a large scale hydrogen furnace for annealing while improving the homogeneity of the shielded region's magnetic field by an order of magnitude compared to the previous work.[15] This opens shielding possibilities for ultra-large scale experiments proposed to detect gravitational waves or search for exotic matter with atomic matter waves[29,30] where monolithic designs cannot be considered. For interferometer geometries using the full length of the baseline, our shield leads to a Zeeman effect associated bias for ^{87}Rb atoms below five parts in 10^{15} of the Earth's local gravitational acceleration. This enables a new class of absolute gravimeters for long-term gravity monitoring and reference networks.[31] Finally, when comparing the acceleration of two different atomic species, this paves the way toward Galilean tests of the universality of free fall with atomic test masses beyond the 10^{-13} level.[13]

ACKNOWLEDGMENTS

The Hannover Very Long Baseline Atom Interferometry facility is a major research facility funded by the German Research Foundation (Deutsche Forschungsgemeinschaft, DFG). This work was supported by the Collaborative Research Centers 1128 "geo-Q" (Project No. A02) and 1227 "DQ-mat" (Project No. B07), and Germany's Excellence Strategy within EXC-2123 "QuantumFrontiers" (Project No. 390837967). D.S. acknowledges funding from the German Federal Ministry of Education and Research (BMBF) through the funding program Photonics Research Germany (Contract No. 13N14875). E.W. acknowledges support from "Niedersächsisches Vorab" through the "Quantum- and Nano-Metrology (QUANOMET)" initiative (Project No. QT3 - 51170991). S.S. and P.F. acknowledge support from EXC-153 "Origin and Structure of the Universe" (Project No. 24799710). The work of C.U. was supported by the German Aerospace Center (DLR) with funds provided by the Federal Ministry for Economic Affairs and Energy (BMWi) due to an enactment of the German Bundestag under Grant Nos. DLR 50WM1556 and 50WM1956. E.W., D.T., E.M.R., and D.S. thank I. Fan and A. Schnabel for valuable insight at the beginning of the project. E.W. thanks T. Wendrich, K. M. Knaak, T. Hensel, and T. Rehmert for logistics help and the loan of measurement equipment.

REFERENCES

[1] G. Rosi, F. Sorrentino, L. Cacciapuoti, M. Prevedelli, and G. Tino, Nature **510**, 518 (2014).
[2] R. Bouchendira, P. Cladé, S. Guellati-Khélifa, F. Nez, and F. Biraben, Phys. Rev. Lett. **106**, 080801 (2011).
[3] R. H. Parker, C. Yu, W. Zhong, B. Estey, and H. Müller, Science **360**, 191 (2018).
[4] K. S. Hardman, P. J. Everitt, G. D. McDonald, P. Manju, P. B. Wigley, M. A. Sooriyabandara, C. C. N. Kuhn, J. E. Debs, J. D. Close, and N. P. Robins, Phys. Rev. Lett. **117**, 138501 (2016).
[5] B. Barrett, L. Antoni-Micollier, L. Chichet, B. Battelier, T. Lévèque, A. Landragin, and P. Bouyer, Nat. Commun. **7**, 13786 (2016).
[6] M. Jaffe, P. Haslinger, V. Xu, P. Hamilton, A. Upadhye, B. Elder, J. Khoury, and H. Müller, Nat. Phys. **13**, 938 (2017).
[7] D. O. Sabulsky, I. Dutta, E. A. Hinds, B. Elder, C. Burrage, and E. J. Copeland, Phys. Rev. Lett. **123**, 061102 (2019).
[8] C. Freier, M. Hauth, V. Schkolnik, B. Leykauf, M. Schilling, H. Wziontek, H.-G. Scherneck, J. Müller, and A. Peters, J. Phys.: Conf. Ser. **723**, 012050 (2016).
[9] P. Gillot, O. Francis, A. Landragin, F. P. Dos Santos, and S. Merlet, Metrologia **51**, L15 (2014).
[10] M. A. Kasevich and S. Chu, Phys. Rev. Lett. **67**, 181 (1991).
[11] T. Kovachy, P. Asenbaum, C. Overstreet, C. A. Donnelly, S. M. Dickerson, A. Sugarbaker, J. M. Hogan, and M. A. Kasevich, Nature **528**, 530 (2015).
[12] L. Zhou, Z. Y. Xiong, W. Yang, B. Tang, W. C. Peng, K. Hao, R. B. Li, M. Liu, J. Wang, and M. S. Zhan, Gen. Relativ. Gravitation **43**, 1931 (2011).
[13] J. Hartwig, S. Abend, C. Schubert, D. Schlippert, H. Ahlers, K. Posso-Trujillo, N. Gaaloul, W. Ertmer, and E. M. Rasel, New J. Phys. **17**, 035011 (2015).
[14] A. Mager, IEEE Trans. Magn. **6**, 67 (1970).
[15] S. M. Dickerson, J. M. Hogan, D. M. S. Johnson, T. Kovachy, A. Sugarbaker, S.-W. Chiow, and M. A. Kasevich, Rev. Sci. Instrum. **83**, 065108 (2012).
[16] I. Altarev, E. Babcock, D. Beck, M. Burghoff, S. Chesnevskaya, T. Chupp, S. Degenkolb, I. Fan, P. Fierlinger, A. Frei, E. Gutsmiedl, S. Knappe-Grüneberg, F. Kuchler, T. Lauer, P. Link, T. Lins, M. Marino, J. McAndrew, B. Niessen, S. Paul, G. Petzoldt, U. Schläpfer, A. Schnabel, S. Sharma, J. Singh, R. Stoepler, S. Stuiber, M. Sturm, B. Taubenheim, L. Trahms, J. Voigt, and T. Zechlau, Rev. Sci. Instrum. **85**, 075106 (2014).
[17] Seamless extrusion of aluminum EN AW 6060, residual pressure below 1×10^{-9} mbar.
[18] Krupp Magnifer 7904.
[19] J. E. Zimmerman, J. Appl. Phys. **48**, 702 (1977).
[20] G. Stroink, B. Blackford, B. Brown, and M. Horacek, Rev. Sci. Instrum. **52**, 463 (1981).
[21] Bartington Instruments, Model MAG-03, 100 μT full range.
[22] Bartington Instruments, Model PSU-1.
[23] Keysight Technologies, Model 34461A.
[24] 50 points with 10 powerline cycle long acquisition windows and the auto-zero feature turned on.
[25] With a 100 μT full scale sensor, 1 nT corresponds to 100 μV, which can easily appear spuriously on a faulty electrical connection.
[26] D. A. Steck, Rubidium 87 D line data, 2015, http://steck.us/alkalidata.
[27] C. Chiu and L. Stodolsky, Phys. Rev. D **22**, 1337 (1980).
[28] C. Ufrecht, "Theoretical approach to high-precision atom interferometry," Ph.D. thesis, Universität, Ulm, 2019.
[29] M.-S. Zhan, J. Wang, W.-T. Ni, D.-F. Gao, G. Wang, L.-X. He, R.-B. Li, L. Zhou, X. Chen, J.-Q. Zhong, B. Tang, Z.-W. Yao, L. Zhu, Z.-Y. Xiong, S.-B. Lu, G.-H. Yu, Q.-F. Cheng, M. Liu, Y.-R. Liang, P. Xu, X.-D. He, M. Ke, Z. Tan, and J. Luo, Int. J. Mod. Phys. D **2019**, 1940005.
[30] J. Coleman, in Proceedings of the 39th International Conference on High-Energy Physics (ICHEP2018), Seoul, Korea, July 2018.
[31] M. Van Camp, O. de Viron, A. Watlet, B. Meurers, O. Francis, and C. Caudron, Rev. Geophys. **55**, 938, https://doi.org/10.1002/2017rg000566 (2017).